

Persistence-Speed Coupling Enhances the Search Efficiency of Migrating Immune Cells

M. Reza Shaebani,^{1,2,*} Robin Jose,¹ Ludger Santen,^{1,2} Luiza Stankevics,³ and Franziska Lautenschläger^{2,3,4}

¹*Department of Theoretical Physics, Saarland University, 66123 Saarbrücken, Germany*

²*Center for Biophysics, Saarland University, 66123 Saarbrücken, Germany*

³*INM-Leibniz Institute for New Materials, 66123 Saarbrücken, Germany*

⁴*Department of Experimental Physics, Saarland University, 66123 Saarbrücken, Germany*

Migration of immune cells within the human body allows them to fulfill their main function of detecting pathogens. Adopting an optimal navigation and search strategy by these cells is of crucial importance to achieve an efficient immune response. Analyzing the dynamics of dendritic cells in our in vitro experiments reveals that the directional persistence of these cells is highly correlated with their migration speed, and that the persistence-speed coupling enables the migrating cells to reduce their search time. We introduce theoretically a new class of random search optimization problems by minimizing the mean first-passage time (MFPT) with respect to the strength of the coupling between influential parameters such as speed and persistence length. We derive an analytical expression for the MFPT in a confined geometry and verify that the correlated motion improves the search efficiency if the mean persistence length $\langle \ell_p \rangle$ is sufficiently shorter than the confinement size. In contrast, a positive persistence-speed correlation even increases the MFPT at long $\langle \ell_p \rangle$ regime, thus, such a strategy is disadvantageous for highly persistent active agents.

A successful immune response crucially depends on its first steps: finding harmful pathogens. In general, search and transport efficiency of random processes have been quantified by observables such as the diffusivity of randomly moving particles [1], the reactivity of transport-limited chemical reactions [2], the cover time to visit all sites of a confined domain [3, 4], or often by the mean first-passage time (MFPT) that a searcher needs to find a target [5, 6]. Optimal search strategies considered so far minimize the MFPT or equivalently the cover time with respect to one of the key parameters of the problem. This can be either a structural property of the environment in which the particle moves [7, 8] or a parameter of the stochastic motion (e.g., the persistency in active random searches [9], the resetting rate in diffusion processes with stochastic resetting to the initial position [10, 11], the ratio between the durations of diffusive and directed motion in intermittent searches [5, 12, 13], or the speed of the searcher when passing over a target location [14]). However, the influential factors governing the search efficiency are correlated in general. For instance, a universal coupling between migration speed and directional persistence has been recently reported for various cell lines mediated by retrograde actin flows [15]. Alternative optimal search strategies for such correlated stochastic processes need to be developed.

Adopting an efficient search and navigation strategy is of particular importance in biological systems as, for example, in search for specific target sites over a DNA strand by proteins [16–18], escape through small absorbing boundaries and targeted intracellular transport [7, 19], delivery of chemical signals in neurons [20–22], bacterial swimming and chemotaxis [5, 23–25], and animal foraging [14, 26, 27]. It is often hypothesized that the motility of mammalian cells enables them to effec-

tively fulfill their biological functions. Migration of immune cells [28–30], which is expected to be optimized in the course of evolution to achieve an efficient immune response, is of particular interest. Nevertheless, the optimality of the search for pathogens and other targets by immune cells has neither been precisely verified nor systematically studied. Understanding the mechanisms of adaptive search and clearance in the immune system opens the way toward more effective cancer immunotherapies and vaccine design.

Here we consider theoretically a correlated stochastic process and introduce, for the first time, a new class of

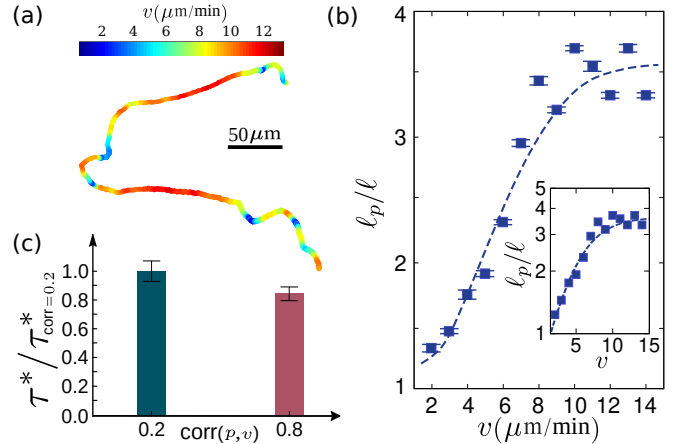


FIG. 1. (a) Sample cell trajectory, color coded with respect to speed. (b) Cell persistence length ℓ_p (scaled by the mean distance ℓ between successive recorded positions) in terms of migration speed v . The dashed line shows the fit via Eq. (1). Inset: Log-linear plot of ℓ_p/ℓ vs v . (c) Comparison between the conditional MFPT τ^* of two categories of cells with low and high p - v correlation.

optimal search strategies based on tuning the strength of coupling between key parameters. Inspired by the observed correlations in the dynamics of dendritic cells [15, 31], we consider the correlation between the migration speed v and directional persistence p of the searcher. The optimization is achieved by analytically calculating the MFPT and minimizing it with respect to the strength κ_{pv} of p - v coupling. The success of the scheme in improving the MFPT nontrivially depends on the ratio between the mean persistence length $\langle \ell_p \rangle$ of the searcher and the system size L ; in the regime $\langle \ell_p \rangle \ll L$ ($\langle \ell_p \rangle \sim L$), the correlated motion is advantageous (disadvantageous) for reducing the search time. We experimentally investigate the dynamics of dendritic cells (responsible for tissue patrolling and antigen capture [30, 32]) and expectedly observe a significant persistence-speed correlation [15, 31] (see Fig. 1). Our data analysis also reveals an interesting inverse dependence of the MFPT on the coupling strength, in agreement with our analytical predictions for the low persistence regime.

Migration of dendritic cells.— To study the dynamics of migrating cells in our in vitro experiments, we tracked the 2D motion of Murine bone marrow-derived immature dendritic cells with typical size of nearly ten micrometers. The motion was confined between the cell culture dish and a roof held by microfabricated pillars made out of Polydimethylsiloxane (PDMS) as described in [33] at a height of $3 \mu\text{m}$. Both surfaces were coated with PLL-PEG (0.5 mg/mL), a non-adhesive material to exclude movement by cell adhesion. The cell concentration was low enough to treat the cells as non-interacting. Cell nuclei were stained with Hoechst 34580 (200 ng/mL for 30 min) (Sigma Aldrich, St Louis, USA) and migration was recorded by epifluorescence microscopy for at least 6h at 37° with a camera of $6.5 \mu\text{m}$ pixel size and sampling rate of 20 frames/h.

A typical cell trajectory is shown in Fig. 1(a), evidencing that the path is more straight when the migration speed is higher. We quantify the cell persistence—the ability of the cell to maintain its current direction of motion— by $p = \cos \theta$ with θ being the orientational change at each recorded position [34–36], from which the instantaneous persistence length ℓ_p can be estimated as $\ell_p = \frac{\ell}{|\ln |p||}$ (ℓ is the mean distance between two successive recorded positions) [37]. The leading contribution in the limit of small θ goes as $\mathcal{O}(\frac{\ell}{1-p})$. After averaging over all trajectories and speed binning intervals of $\Delta v = 1 \mu\text{m}/\text{min}$, we observe a clear coupling between the cell persistence p and the migration speed v , which can be fitted by an exponential saturation $p = p_\infty (1 - e^{-\gamma v})$, with $p_\infty \approx 0.7$ and $\gamma \approx 0.3$. The behavior of ℓ_p is well fitted by a logistic function

$$\ell_p = \frac{\ell_{p_\infty}}{1 + \left(\frac{\ell_{p_\infty} - \ell_{p_0}}{\ell_{p_0}}\right) e^{-\gamma v}}, \quad (1)$$

where ℓ_{p_0} is the persistence length of a nonpersistent motion and $\ell_{p_\infty} \simeq \frac{\ell_{p_0}}{1-p_\infty}$ [Fig. 1(b)]. ℓ_p initially grows exponentially as $\ell_p \propto e^{\gamma v}$ [15] but eventually saturates to ℓ_{p_∞} at high speeds. To describe the overall coupling strength for individual cells we calculate the p - v correlation coefficient $\text{corr}(p, v) = \frac{\text{cov}(p, v)}{\sigma_p \sigma_v}$ for each cell. When averaged over all trajectories, a strong correlation around 0.9 is obtained.

The key question is whether such a correlated random motion helps the immune cells to improve their search efficiency. To answer this, we selected two subpopulations of cells with distinct mean correlation coefficients 0.2 ± 0.05 and 0.8 ± 0.05 . By calculating the conditional MFPT τ^* — i.e. over successful trials to reach a random hidden target— per unit area for each category (scaled by their mean speeds) and various target sizes we obtain 10–15% lower search times at higher correlations, as shown in Fig. 1(c). In order to understand these MFPT results we develop a stochastic model for correlated persistent search in the following, and prove that p - v coupling strategy is only beneficial for relatively weak persistencies, as in the case of dendritic cells.

Correlated persistent search model.— We consider a discrete-time persistent random walk on a two-dimensional square lattice of size L with periodic boundary conditions [Fig. 2(a)]. At each time step, the searcher moves v steps drawn from a speed distribution $f(v)$. It

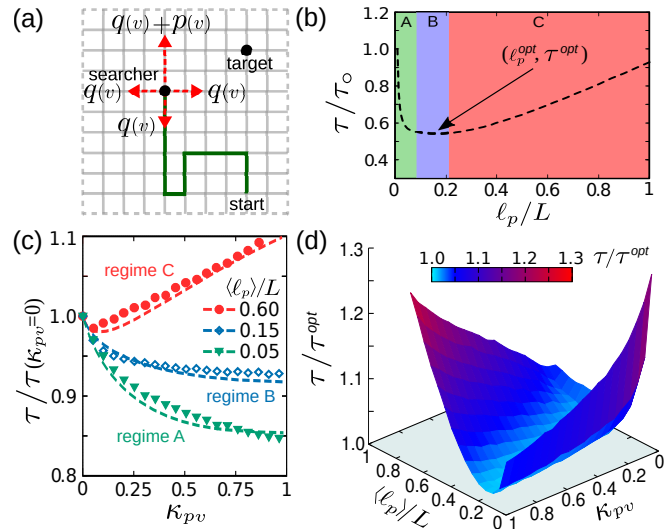


FIG. 2. (a) Sketch of the correlated persistent random search on a square lattice. (b) MFPT of a constant ℓ_p and v process, scaled by the MFPT of a diffusive searcher, vs ℓ_p normalized by L ($L=200$). (c) MFPT of a correlated p - v process, scaled by the MFPT when $\kappa_{pv}=0$, vs the coupling strength κ_{pv} . Each curve belongs to a different regime of $\langle \ell_p \rangle$ shown in panel (b). The dashed lines represent analytical predictions and the symbols are simulation results. (d) MFPT scaled by the optimal search time of the constant ℓ_p process vs κ_{pv} and scaled $\langle \ell_p \rangle$.

either continues along the previous direction of motion with probability $q+p$ or chooses a new direction, each with a probability q , so that $4q+p=1$. The persistency parameter p (and thus q) depends on the instantaneous speed v and ranges from 0 (ordinary diffusion) to 1 (ballistic motion). The instantaneous persistence length can be obtained as $\ell_p = \sum_{\ell=1}^{\infty} \ell(q+p)^{\ell-1}(1-q-p) = \frac{4}{3} \frac{1}{1-p(v)}$.

Assuming that a single target of one lattice-unit size is located at \mathbf{r}_T (equivalent to regularly spaced targets on an infinite plane with $\frac{1}{L^2}$ density), we introduce $\tau(\mathbf{r}, v, \sigma)$ as the MFPT of reaching the target starting at position $\mathbf{r} (\neq \mathbf{r}_T)$ with speed v and orientation $\sigma \in \{\rightarrow, \leftarrow, \uparrow, \downarrow\}$. The evolution of $\tau(\mathbf{r}, v, \sigma)$ can be described by the following backward master equation

$$\tau(\mathbf{r}, v, \rightarrow) = \int dv' f(v') \left[(q+p) \tau(\mathbf{r} + v\hat{\mathbf{i}}, v', \rightarrow) + q \tau(\mathbf{r} - v\hat{\mathbf{i}}, v', \leftarrow) + q \tau(\mathbf{r} + v\hat{\mathbf{j}}, v', \uparrow) + q \tau(\mathbf{r} - v\hat{\mathbf{j}}, v', \downarrow) + 1 \right], \quad (2)$$

and similar master equations for $\tau(\mathbf{r}, v, \leftarrow)$, $\tau(\mathbf{r}, v, \uparrow)$ and $\tau(\mathbf{r}, v, \downarrow)$. The possible velocities are limited to the integer values $v' \in [0, v_{\max}]$, which are supposed to be equally probable for simplicity. By introducing the Fourier transform $\tau(\mathbf{k}, v, \sigma) = \sum_{\mathbf{r}} \tau(\mathbf{r}, v, \sigma) e^{-i\mathbf{k} \cdot \mathbf{r}}$ and using $\int dv' f(v') \tau(\mathbf{k}, v, \sigma) = \tau(\mathbf{k}, \sigma)$ for a uniform distribution $f(v)$, after some calculations we obtain

$$\tau(\mathbf{k}, \sigma) = \frac{F(\mathbf{k}) + S(\delta(\mathbf{k}) - e^{-i\mathbf{k} \cdot \mathbf{r}_T})}{1 - B_{\sigma}(\mathbf{k})}, \quad (3)$$

with $B_{\sigma}(\mathbf{k}) = \frac{1}{L} \sum_{v=0}^{v_{\max}} p(v) e^{ivk_{\sigma}}$, $F(\mathbf{k}) = \frac{1}{L} \sum_v p(v) \sum_{\sigma} e^{ivk_{\sigma}} \tau(\mathbf{k}, \sigma)$, $S = L^2$, and $k_{\sigma} \in \{\mathbf{k} \cdot \hat{\mathbf{i}}, -\mathbf{k} \cdot \hat{\mathbf{i}}, \mathbf{k} \cdot \hat{\mathbf{j}}, -\mathbf{k} \cdot \hat{\mathbf{j}}\}$. Next we multiply Eq. (3) by $e^{ivk_{\sigma}}$ and sum over σ and v to derive a closed expression

$$F(\mathbf{k}) = \frac{A(\mathbf{k}) S(\delta(\mathbf{k}) - e^{-i\mathbf{k} \cdot \mathbf{r}_T})}{1 - A(\mathbf{k})}. \quad (4)$$

Here $A(\mathbf{k}) = \frac{1}{L} \sum_v p(v) \sum_{\sigma} \frac{e^{ivk_{\sigma}}}{1 - B_{\sigma}(\mathbf{k})}$. Inserting $F(\mathbf{k})$ into Eq. (3) and averaging over all directions σ then yields

$$\tau(\mathbf{k}) = \frac{C(\mathbf{k}) S(\delta(\mathbf{k}) - e^{-i\mathbf{k} \cdot \mathbf{r}_T})}{1 - A(\mathbf{k})}, \quad (5)$$

where $C(\mathbf{k}) = \frac{1}{4} \sum_{\sigma} \frac{1}{1 - B_{\sigma}(\mathbf{k})}$. Finally, we apply the inverse Fourier transform (with the components of available modes being $k_i = \frac{2\pi n_i}{L}$, $n_i \in [0, L-1]$) and numerically average over all possible starting positions \mathbf{r} to obtain the overall MFPT τ .

In the case of constant persistence and speed, the results of a single-state persistent random search [9] are

recovered, where the MFPT shows a minimum τ^{opt} at an optimal persistence length ℓ_p^{opt} ; see Fig. 2(b). The optimal value $\frac{\ell_p^{\text{opt}}}{L}$ slightly decreases with increasing L . For correlated random searches, we consider a linear relation between ℓ_p and v for simplicity, corresponding to an expansion of Eq. (1) up to the first order term in v . We use

$$\frac{\ell_p}{\langle \ell_p \rangle} = \kappa_{pv} (\tilde{v} - 1) + 1, \quad (6)$$

with \tilde{v} being the scaled speed $\tilde{v} = \frac{v}{\langle v \rangle}$ and κ_{pv} the strength of persistence-speed coupling. The persistence length ℓ_p equals $\langle \ell_p \rangle$ for zero coupling coefficient and ranges within $[0, 2\langle \ell_p \rangle]$ for $\kappa_{pv} = 1$. By inserting the resulting persistence parameter $p(v)$ in the above formalism, we obtain $\tau(\langle \ell_p \rangle, \kappa_{pv})$. We checked that using Eq. (1) instead of Eq. (6) yields qualitatively analogous results to those reported in the following.

Combined effects of $\langle \ell_p \rangle$ and κ_{pv} on search efficiency.— Interestingly, Fig. 2(c) reveals different dependencies of the MFPT on the coupling strength κ_{pv} for choices of $\langle \ell_p \rangle$ taken from low, intermediate, and high persistence-length regimes A, B, C, as specified in Fig. 2(b). While τ is a decreasing function of κ_{pv} at low $\langle \ell_p \rangle$, the search efficiency at high mean persistence lengths even reduces with increasing κ_{pv} . Compared with the optimal choice of the constant persistence length strategy, the $p-v$ correlated search is always less efficient but approaches the search time τ^{opt} of the former strategy at $\langle \ell_p \rangle$ values around ℓ_p^{opt} ; see Fig. 2(d). Note that even at $\kappa_{pv} = 0$ the two strategies are not equivalent as the velocity is a variable quantity in the correlated search strategy (uniformly distributed within $[0, 2\langle v \rangle]$). The fact that the search time for the optimal choice of constant persistence length ℓ_p^{opt} is the absolute minimum over all correlated and uncorrelated persistent searches provides a qualitative explanation for the observed behavior in correlated random searches; inducing $p-v$ coupling at low $\langle \ell_p \rangle$ regime A

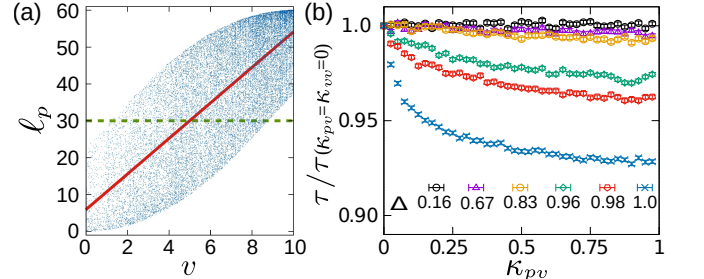


FIG. 3. (a) Example of correlated (v, ℓ_p) pairs generated in simulations with the coupling strength $\kappa_{pv} = 0.8$, drawn from a distribution with $\langle \ell_p \rangle = 30$ (dashed line) and width $\Delta = 1$. The solid line represents the $p-v$ coupling according to Eq. (6). $L = 200$. (b) Influence of the distribution width Δ on the MFPT as a function of the coupling strength κ_{pv} .

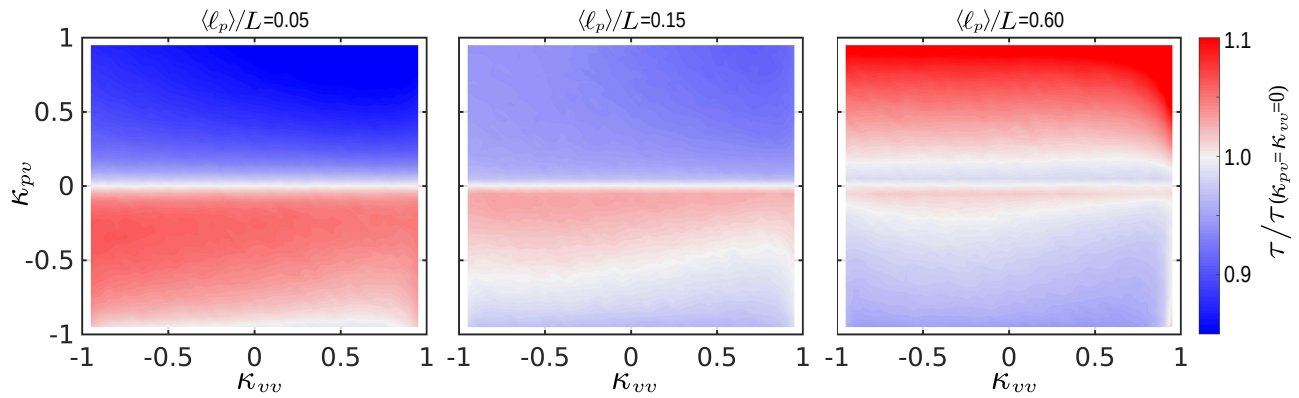


FIG. 4. Phase diagram of the MFPT in $(\kappa_{vv}, \kappa_{pv})$ plane for different values of mean persistence length $\langle \ell_p \rangle$. The search time of an uncorrelated $p-v$ process in the absence of speed autocorrelations $\tau(\kappa_{vv}=\kappa_{pv}=0)$ is taken as the reference for comparison in each panel. The color intensity indicates the deviation from the uncorrelated-search time, with red (blue) reflecting a decrease (increase) in the search efficiency.

helps to effectively increase the persistence of motion i.e. toward ℓ_p^{opt} . This is in sharp contrast to the high $\langle \ell_p \rangle$ regime C where the increase of effective persistence length by $p-v$ correlations drags it away from ℓ_p^{opt} leading to a less efficient search. In the plateau regime B the $p-v$ coupling is expectedly less influential. We can analytically verify a distinct dependency of τ on κ_{pv} at two extreme regimes $\langle \ell_p \rangle \rightarrow 0$ and $\langle \ell_p \rangle \rightarrow L$: Up to the leading order term, τ increases linearly with κ_{pv} at high persistency as $\tau(\langle \ell_p \rangle \rightarrow L) \sim \frac{1}{1-p} = a_1 \langle \ell_p \rangle \kappa_{pv} + a_2$; however, it decreases inversely with κ_{pv} when the persistency is extremely low, where it can be shown that $\tau(\langle \ell_p \rangle \rightarrow 0) \sim \frac{1-p}{1+p} = \frac{1}{b_1 \langle \ell_p \rangle \kappa_{pv} + b_2}$ ($a_1, b_1 > 0$).

Speed autocorrelation.— So far we analytically obtained the MFPT in the presence of persistence-speed correlation for a randomly varying speed at each time step. However, the successive instantaneous speeds can be correlated in general such that the searcher experiences a rather smooth speed change over time. For instance, we obtain a positive speed autocorrelation coefficient $\kappa_{vv} \approx 0.3$ for the dendritic cells in our experiments. To incorporate the speed autocorrelation in our analytical approach, one should replace the speed distribution $f(v')$ in the master equation (2) with the probability distribution of speed change $f(v-v')$. Analytical determination of the MFPT for autocorrelated speed however appears to be intractable; thus, we resort to Monte Carlo simulations to generate the desired stochastic motion.

In our simulations, we use the *sum-of-uniforms* algorithm [38–40] to correlate speed and persistence length and to include speed autocorrelation. The algorithm allows for inducing a certain degree of stochasticity in the resulting v and ℓ_p values, which is controlled by an additional parameter Δ . At each time step, first a new speed is chosen from a distribution around the current speed, which generates the demanded speed autocorrelation κ_{vv} . Then a new ℓ_p is chosen from a uniform distri-

bution of ℓ_p values around the value determined by the $p-v$ coupling strength κ_{pv} and the local speed v according to Eq. (6) [red line in Fig. 3(a)]. This results in the cloud of blue dots in the figure. The parameter $\Delta \in [0, 1]$ tunes the actual slope of the cloud (the upper limit is however set by κ_{pv}) and allows for $\pm \Delta \langle \ell_p \rangle$ overall fluctuations. As shown in Fig. 3(b), τ approaches the MFPT of uncorrelated motion by decreasing the scattering parameter Δ . Here we show the simulation results for $\Delta=1$ corresponding to the widest overall range of persistence length $[0, 2\langle \ell_p \rangle]$. Once the new v and ℓ_p are determined, we extract the instantaneous persistence p of the searcher and move it v sub-steps within one time step by allowing it to change the direction of motion after each sub-step according to the persistence probability p .

The results of uncorrelated speeds $\kappa_{vv}=0$ in different regimes of $\langle \ell_p \rangle$ are shown in Fig. 2(c); the agreement between analytical predictions and simulation results is satisfactory. When speed autocorrelations are switched on, we find that the trends reported in Fig. 2(c) remain qualitatively valid. κ_{vv} plays a relatively insignificant role in determining the search time, while $\langle \ell_p \rangle$ and κ_{pv} are influential factors. We extend the range of correlation coefficients κ_{pv} and κ_{vv} to negative values for anti-correlated dynamics. Figure 4 summarizes the results in a phase diagram of search times in $(\kappa_{vv}, \kappa_{pv})$ plane. τ shows only modest dependence on κ_{vv} (subtle color intensity changes along horizontal lines) but variation of κ_{pv} may cause even up to 25% changes in the search time. Another point is that inducing $p-v$ anticorrelation reduces the effective persistence of motion, thus, acts in the opposite direction, i.e. it improves the search time in regime C while leads to an increased search time in regime A.

Immature dendritic cells are located in the interstitial space of peripheral tissues. In the skin, for example, the dermal dendritic cells are present in a high density of a few hundred cells per mm^2 [41]. If each dendritic

cell patrols, on average, an area of linear size $L \sim 100 \mu\text{m}$ with a persistence length of less than $10 \mu\text{m}$ (for typical speeds of $3\text{--}4 \mu\text{m}/\text{min}$ and assuming even a high persistence $p \approx 0.7$ before reaching the $p\text{--}v$ saturation regime), then these cells belong to the weakly persistent regime A in Fig. 2(b) (indeed regime A is even more extended to right for such small patrolling areas). In small intrapulmonary airways, the density of dendritic cells is less than a hundred per mm^2 in the absence of inflammation [42]. In such regions, each cell is responsible for patrolling a larger area and the corresponding relative persistence length in Fig. 2(b) further shifts to the left in zone A. As a result, $p\text{--}v$ correlations are beneficial for immature dendritic cells to improve the search efficiency in various biological environments.

In summary, our study suggests improving the search efficiency of an active agent by inducing persistence-speed correlations and/or speed autocorrelations. Our key finding is that a correlated random motion is not necessarily an optimal search strategy in general; it is advantageous for dendritic cells moving with a persistence length much smaller than the size of the environment, however, highly persistent active agents should even adopt an anticorrelation between their speed and directional persistence to reduce their search time. By optimizing the search efficiency with respect to the strength of coupling between influential parameters, we introduced a new class of random search optimization problems with broad application to correlated stochastic processes such as chemotaxis and chemokinesis dynamics.

This work was funded by the Deutsche Forschungsgemeinschaft (DFG) through Collaborative Research Center SFB 1027. We would like to thank A. M. Lennon Duménil for support with the dendritic cell system and Raphael Voituriez for discussions. M. R. S. and R. J. contributed equally.

* corresponding author. shaebani@lusi.uni-sb.de

- [1] T. Bertrand, Y. Zhao, O. Bénichou, J. Tailleur, and R. Voituriez, *Phys. Rev. Lett.* **120**, 198103 (2018).
- [2] C. Loverdo, O. Bénichou, M. Moreau, and R. Voituriez, *Nat. Phys.* **4**, 134 (2008).
- [3] M. Chupeau, O. Bénichou, and R. Voituriez, *Phys. Rev. E* **89**, 062129 (2014).
- [4] M. Chupeau, O. Bénichou, and R. Voituriez, *Nat. Phys.* **11**, 844 (2015).
- [5] O. Bénichou, C. Loverdo, M. Moreau, and R. Voituriez, *Rev. Mod. Phys.* **83**, 81 (2011).
- [6] S. Redner, *A Guide to First-Passage Processes* (Cambridge University Press, Cambridge, 2001).
- [7] K. Schwarz, Y. Schröder, B. Qu, M. Hoth, and H. Rieger, *Phys. Rev. Lett.* **117**, 068101 (2016).
- [8] M. R. Shaebani, R. Jose, C. Sand, and L. Santen, *Phys. Rev. E* **98**, 042315 (2018).
- [9] V. Tejedor, R. Voituriez, and O. Bénichou, *Phys. Rev. Lett.* **108**, 088103 (2012).
- [10] M. R. Evans and S. N. Majumdar, *Phys. Rev. Lett.* **106**, 160601 (2011).
- [11] L. Kusmierz, S. N. Majumdar, S. Sabhapandit, and G. Schehr, *Phys. Rev. Lett.* **113**, 220602 (2014).
- [12] O. Bénichou, M. Coppey, M. Moreau, P.-H. Suet, and R. Voituriez, *Phys. Rev. Lett.* **94**, 198101 (2005).
- [13] C. Loverdo, O. Bénichou, M. Moreau, and R. Voituriez, *Phys. Rev. E* **80**, 031146 (2009).
- [14] D. Campos, V. Méndez, and F. Bartumeus, *Phys. Rev. Lett.* **108**, 028102 (2012).
- [15] P. Maiuri, J.-F. Rupprecht, S. Wieser, V. Rupprecht, O. Bénichou, N. Carpi, M. Coppey, S. D. Beco, N. Gov, C.-P. Heisenberg, et al., *Cell* **161**, 374 (2015).
- [16] M. A. Lomholt, T. Ambjörnsson, and R. Metzler, *Phys. Rev. Lett.* **95**, 260603 (2005).
- [17] J. Elf, G.-W. Li, and X. S. Xie, *Science* **316**, 1191 (2007).
- [18] M. Bauer and R. Metzler, *Biophys. J.* **102**, 2321 (2012).
- [19] Z. Schuss, A. Singer, and D. Holcman, *Proc. Natl. Acad. Sci. USA* **104**, 16098 (2007).
- [20] P. C. Bressloff and B. A. Earnshaw, *Phys. Rev. E* **75**, 041915 (2007).
- [21] R. Jose, L. Santen, and M. R. Shaebani, *Biophys. J.* **115**, 2014 (2018).
- [22] S. Fedotov and V. Méndez, *Phys. Rev. Lett.* **101**, 218102 (2008).
- [23] J. Najafi, M. R. Shaebani, T. John, F. Altegoer, G. Bange, and C. Wagner, *Sci. Adv.* **4**, eaar6425 (2018).
- [24] G. H. Wadhams and J. P. Armitage, *Nat. Rev. Mol. Cell Biol.* **5**, 1024 (2004).
- [25] E. Perez Ipiña, S. Otte, R. Pontier-Bres, D. Czerucka, and F. Peruani, *Nat. Phys.* **15**, 610 (2019).
- [26] F. Bartumeus and S. A. Levin, *Proc. Natl. Acad. Sci. USA* **105**, 19072 (2008).
- [27] G. Oshanin, O. Vasilyev, P. L. Krapivsky, and J. Klafter, *Proc. Natl. Acad. Sci. USA* **106**, 13696 (2009).
- [28] T. H. Harris, E. J. Banigan, D. A. Christian, C. Konradt, E. D. Tait Wojno, K. Norose, E. H. Wilson, B. John, W. Weninger, A. D. Luster, et al., *Nature* **486**, 545 (2012).
- [29] I. Lavi, M. Piel, A.-M. Lennon-Duménil, R. Voituriez, and N. S. Gov, *Nat. Phys.* **12**, 1146 (2016).
- [30] M. Chabaud, M. L. Heuzé, M. Bretou, P. Vargas, P. Maiuri, P. Solanes, M. Maurin, E. Terriac, M. Le Berre, D. Lankar, et al., *Nat. Commun.* **6**, 7526 (2015).
- [31] P.-H. Wu, A. Giri, S. X. Sun, and D. Wirtz, *Proc. Natl. Acad. Sci. USA* **111**, 3949 (2014).
- [32] M. L. Heuzé, P. Vargas, M. Chabaud, M. Le Berre, Y.-J. Liu, O. Collin, P. Solanes, R. Voituriez, M. Piel, and A.-M. Lennon-Duménil, *Immunol. Rev.* **256**, 240 (2013).
- [33] M. L. Berre, E. Zlotek-Zlotkiewicz, D. Bonazzi, F. Lautenschlaeger, and M. Piel, *Method. Cell Biol.* **121**, 213 (2014).
- [34] M. R. Shaebani, Z. Sadjadi, I. M. Sokolov, H. Rieger, and L. Santen, *Phys. Rev. E* **90**, 030701 (2014).
- [35] Z. Sadjadi, M. R. Shaebani, H. Rieger, and L. Santen, *Phys. Rev. E* **91**, 062715 (2015).
- [36] S. Burov, S. M. A. Tabei, T. Huynh, M. P. Murrell, L. H. Philipson, S. A. Rice, M. L. Gardel, N. F. Scherer, and A. R. Dinner, *Proc. Natl. Acad. Sci. USA* **110**, 19689 (2013).
- [37] M. R. Shaebani and Z. Sadjadi, arXiv e-prints p. arXiv:1909.05033 (2019).

- [38] V. C. Lakhan, *J. Stat. Comput. Simul.* **12**, 303 (1981).
- [39] R. T. Willemain and A. P. Desautels, *J. Stat. Comput. Simul.* **45**, 23 (1993).
- [40] J.-T. Chen, *Eur. J. Oper. Res.* **167**, 226 (2005).
- [41] L. G. Ng, A. Hsu, M. A. Mandell, B. Roediger, C. Hoeller, P. Mrass, A. Iparraguirre, L. L. Cavanagh, J. A. Triccas, S. M. Beverley, et al., *PLOS Pathog.* **4**, e1000222 (2008).
- [42] M. A. Schon-Hegrad, J. Oliver, P. G. McMenamin, and P. G. Holt, *J. Exp. Med.* **173**, 1345 (1991).